

## **Constructing electronic interconnected bimetallic selenides-filled porous carbon nanosheets for stable and highly efficient sodium-ion half/full batteries**

Lei Zhang<sup>a, c</sup>, Xiao Li<sup>c</sup>, Linlin Tai<sup>c</sup>, Chunping Shen<sup>d</sup>, Jun Yang<sup>b\*</sup>, Chencheng Sun<sup>a\*</sup>, Hongbo Geng<sup>c\*</sup>, Xiaobing Zuo<sup>c</sup>

<sup>a</sup>School of Electronic and Information Engineering, Changshu Institute of Technology, Changshu 215500, Jiangsu, China

<sup>b</sup>School of Material Science & Engineering, Jiangsu University of Science and Technology, Zhenjiang, 212003, China

<sup>c</sup>School of Materials Engineering, Changshu Institute of Technology, Changshu, Jiangsu 215500, China

<sup>d</sup>Jiangsu Tenpower Lithium Co., Ltd., Zhangjiagang, Jiangsu, China

E-mail address: iamjyang@just.edu.cn; ccsun@cslg.edu.cn; hbgeng@cslg.edu.cn.

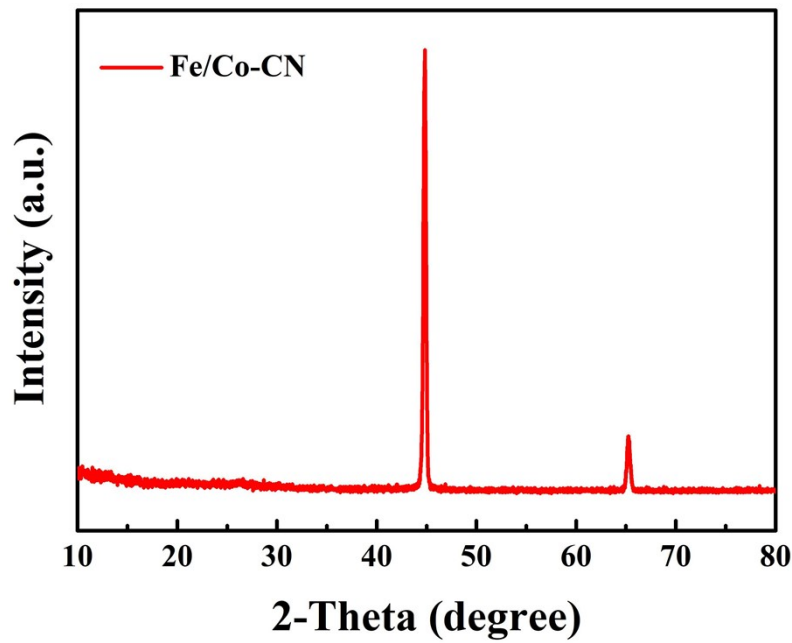


**Figure S1.** XRD pattern of Fe/Co-CN precursor.

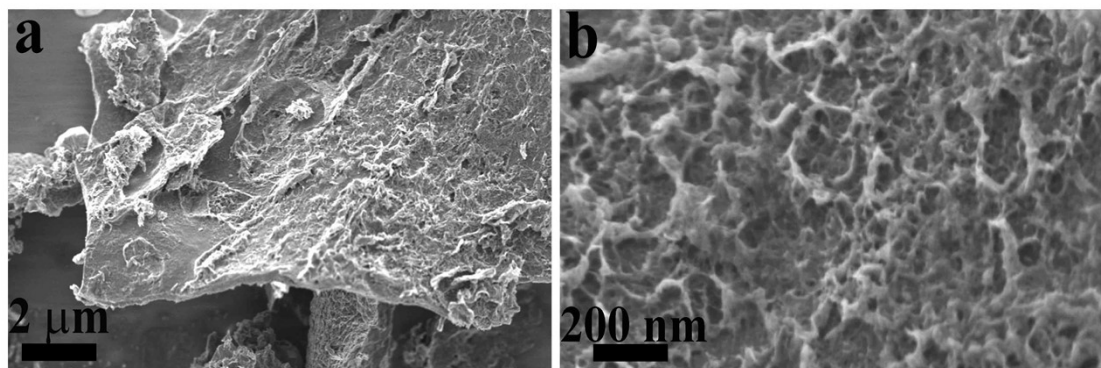


**Figure S2.** (a, b) SEM image of Fe/Co-CN precursor.

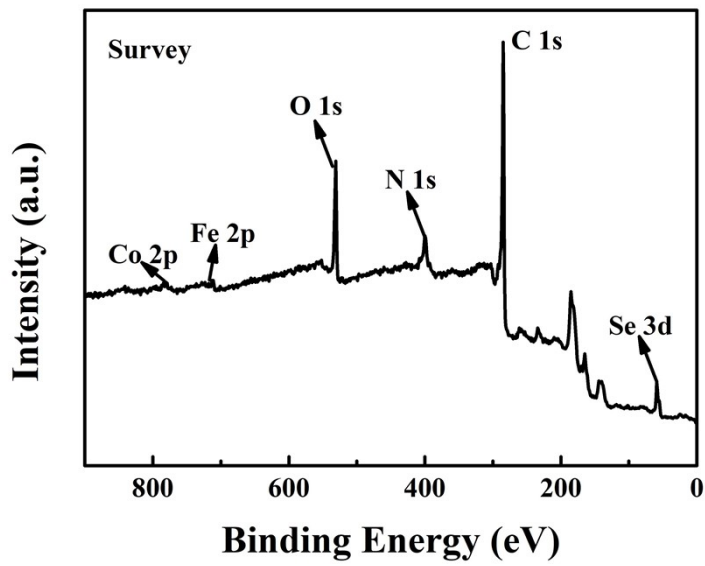


**Figure S3.** XPS spectra of  $\text{FeSe}_2/\text{CoSe}_2\text{-CN}$ .

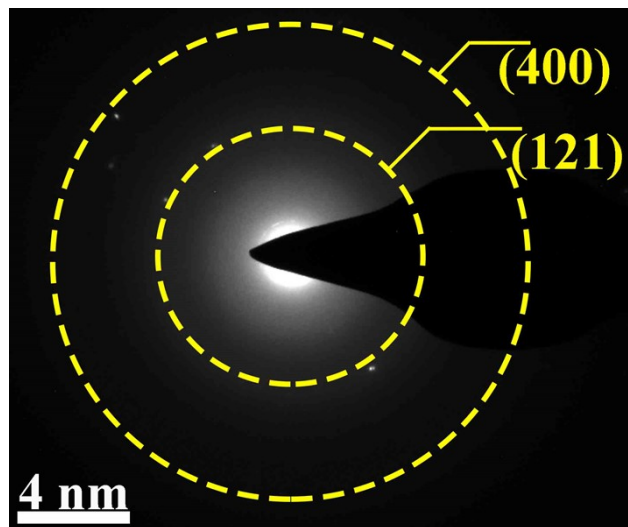


**Figure S4.** SAED pattern of  $\text{FeSe}_2/\text{CoSe}_2\text{-CN}$ .

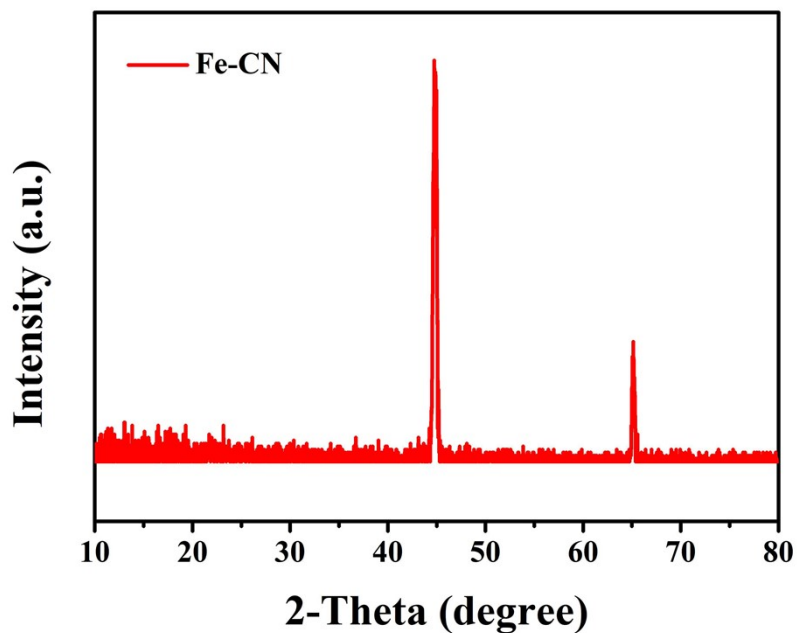


**Figure S5.** XRD pattern of Fe-CN precursor.

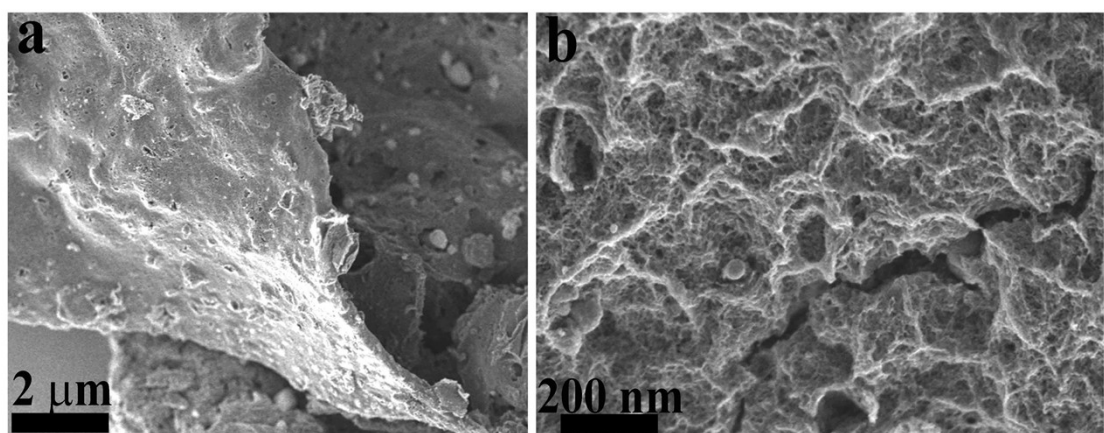


**Figure S6.** (a, b) SEM image of Fe-CN precursor.

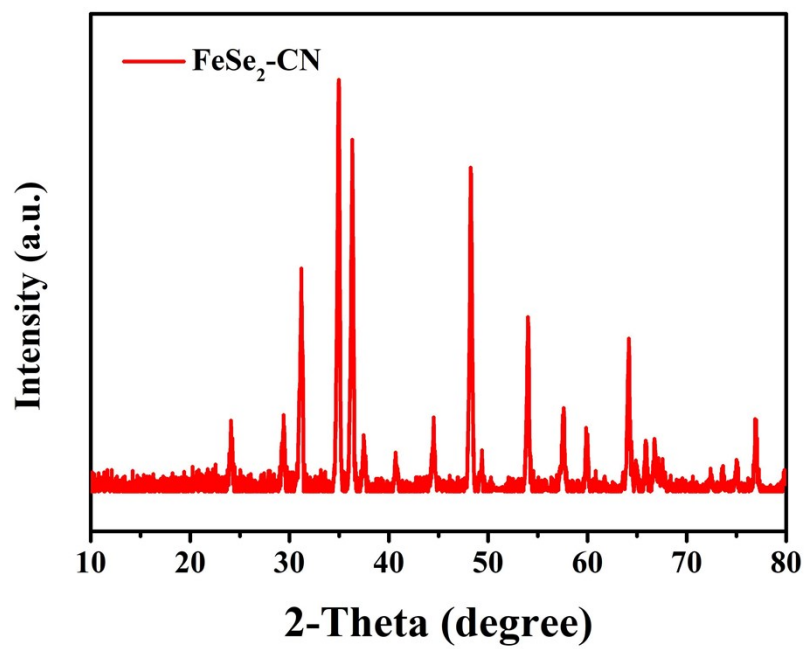


**Figure S7.** XRD pattern of FeSe<sub>2</sub>-CN.

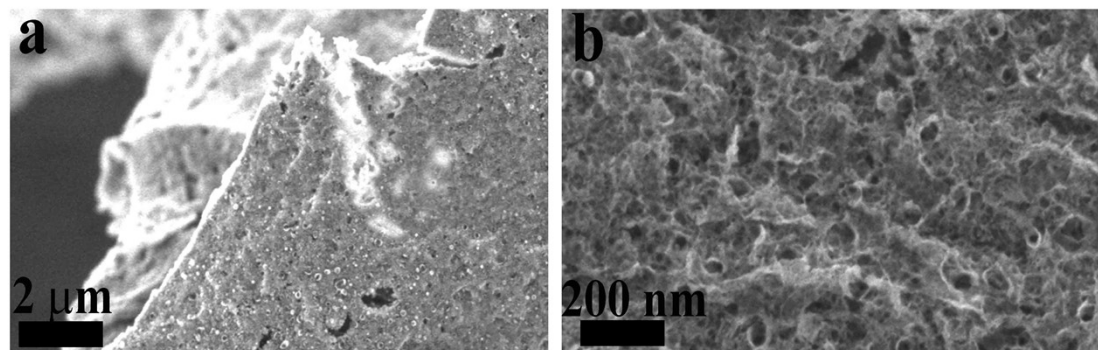


**Figure S8.** (a, b) SEM image of FeSe<sub>2</sub>-CN.

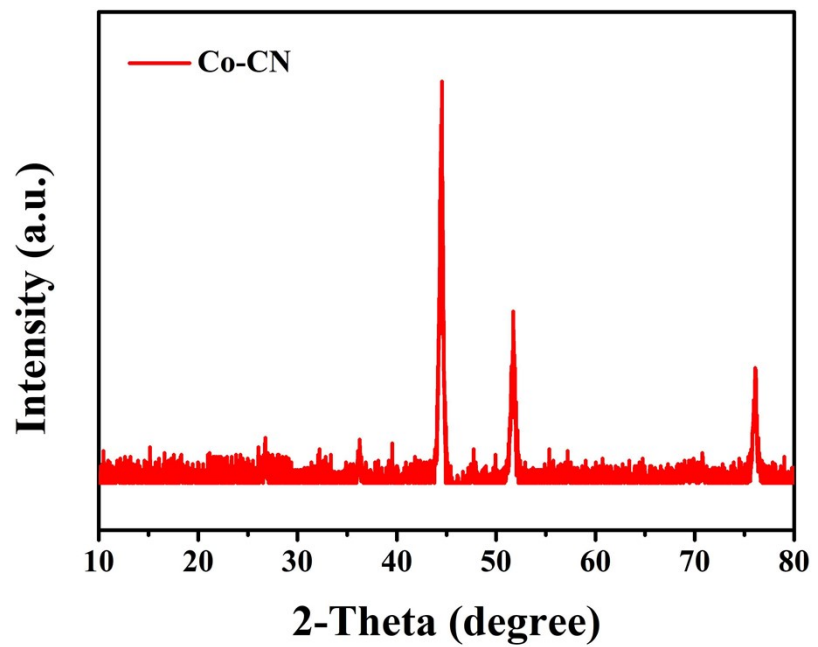


**Figure S9.** XRD pattern of Co-CN precursor.

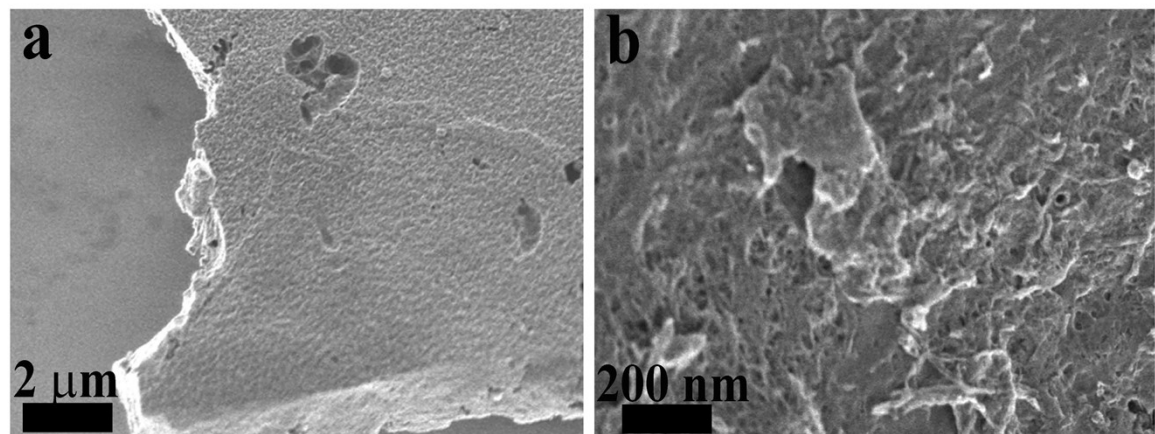


**Figure S10.** (a, b) SEM images of Co-CN precursor.

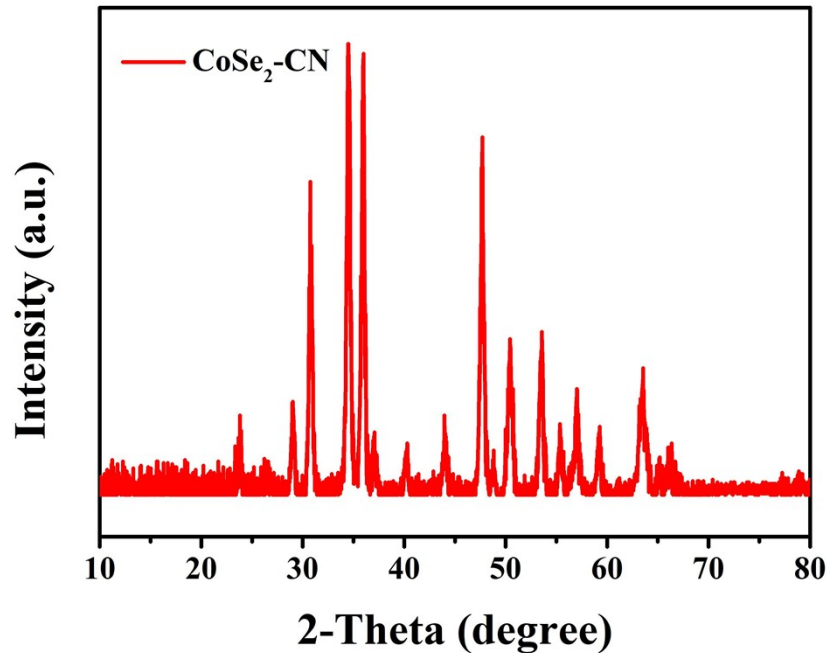


**Figure S11.** XRD pattern of  $\text{CoSe}_2\text{-CN}$ .

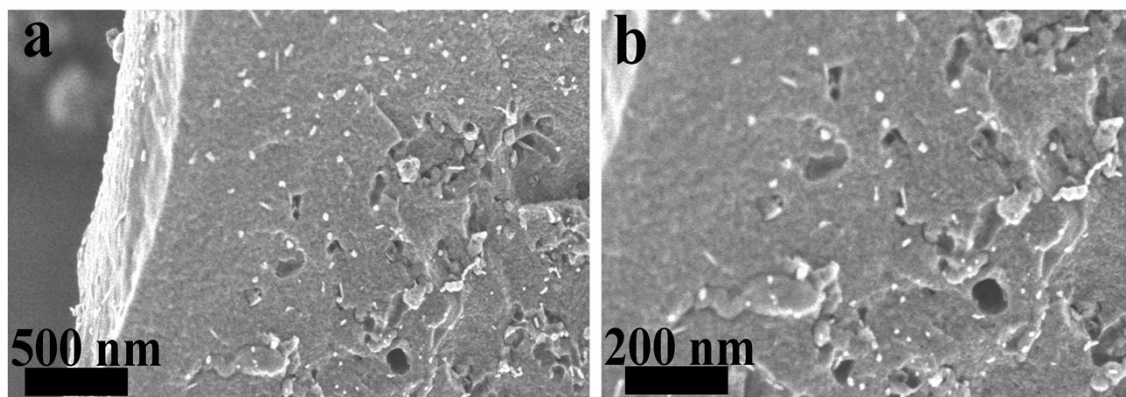


**Figure S12.** (a,b) SEM image of  $\text{CoSe}_2\text{-CN}$ .

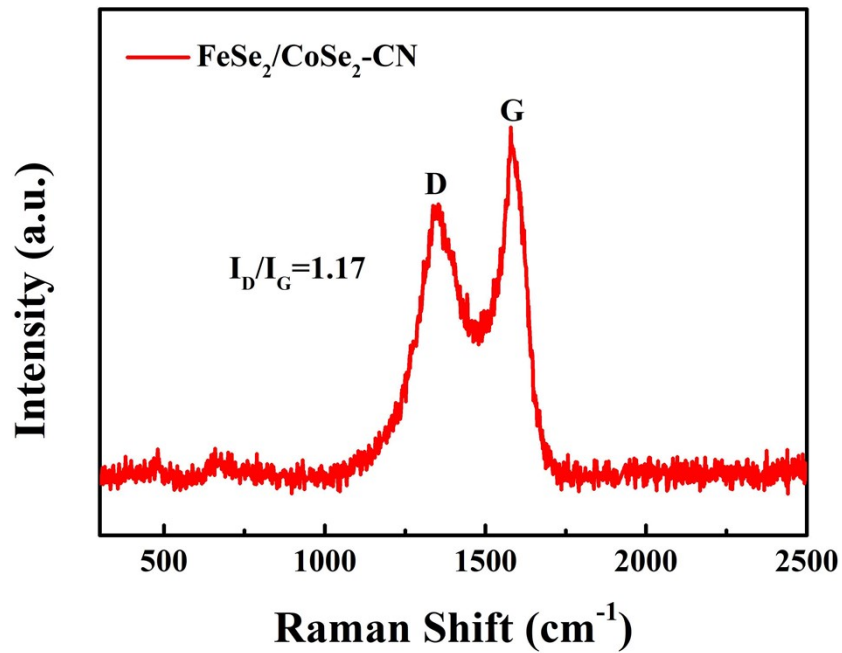


**Figure S13.** Raman spectrum of  $\text{FeSe}_2/\text{CoSe}_2\text{-CN}$ .

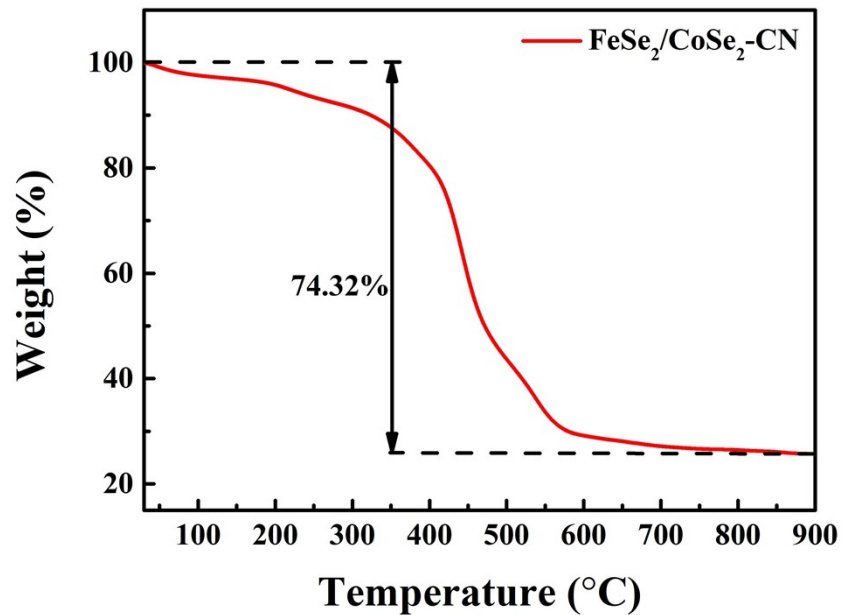


**Figure S14.** TGA curve of  $\text{FeSe}_2/\text{CoSe}_2\text{-CN}$ .

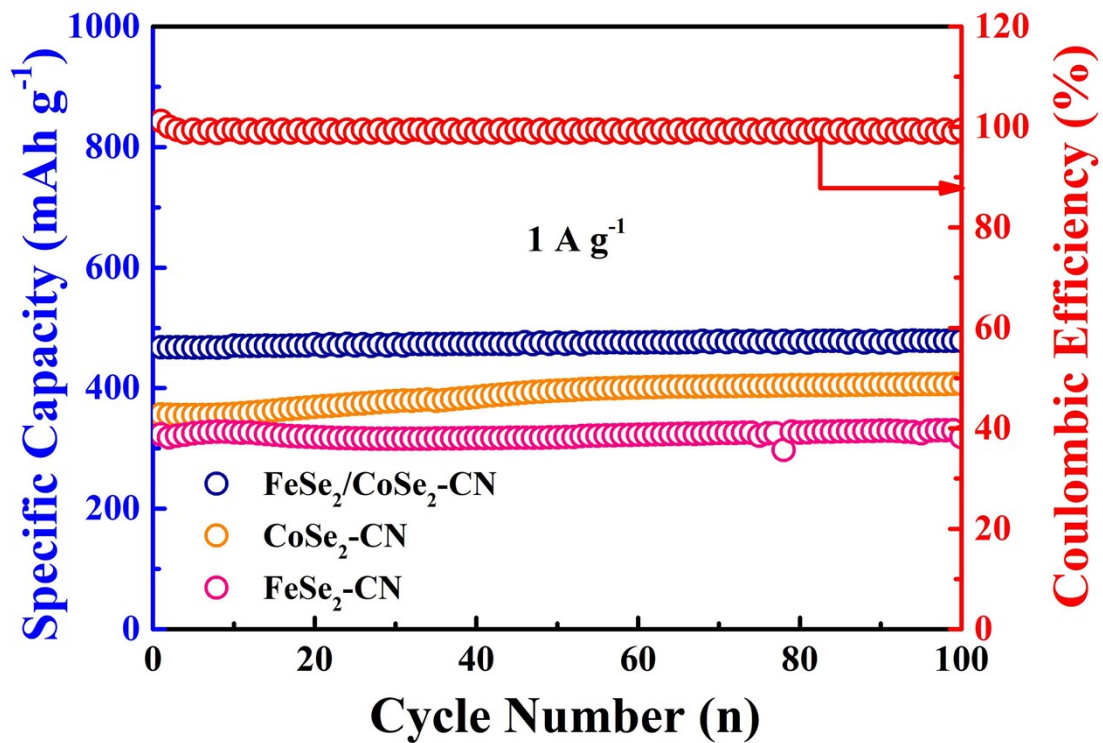


**Figure S15.** The stability comparison of  $\text{FeSe}_2/\text{CoSe}_2\text{-CN}$ ,  $\text{FeSe}_2\text{-CN}$  and  $\text{CoSe}_2\text{-CN}$  at  $1 \text{ A g}^{-1}$ .

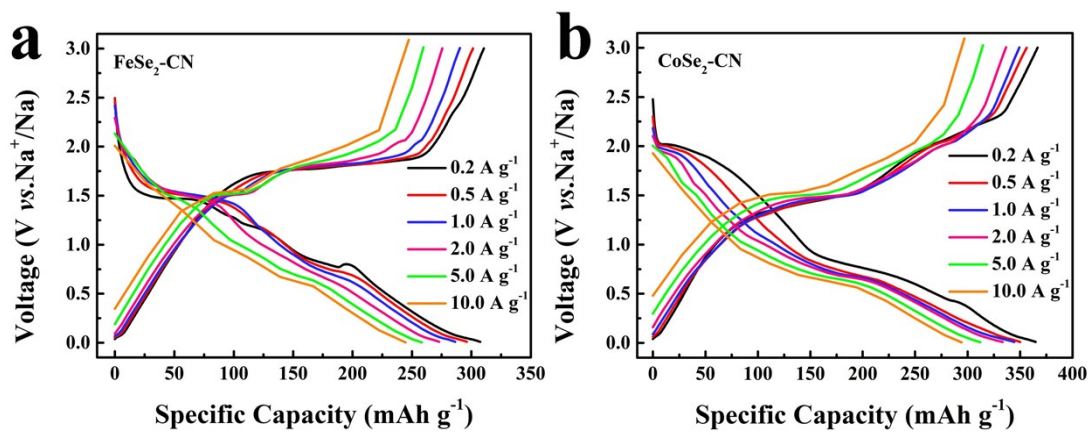


**Figure S16.** The discharge-charge curves of (a) FeSe<sub>2</sub>-CN and (b) CoSe<sub>2</sub>-CN at various current densities from 0.2 to 10 A g<sup>-1</sup>.

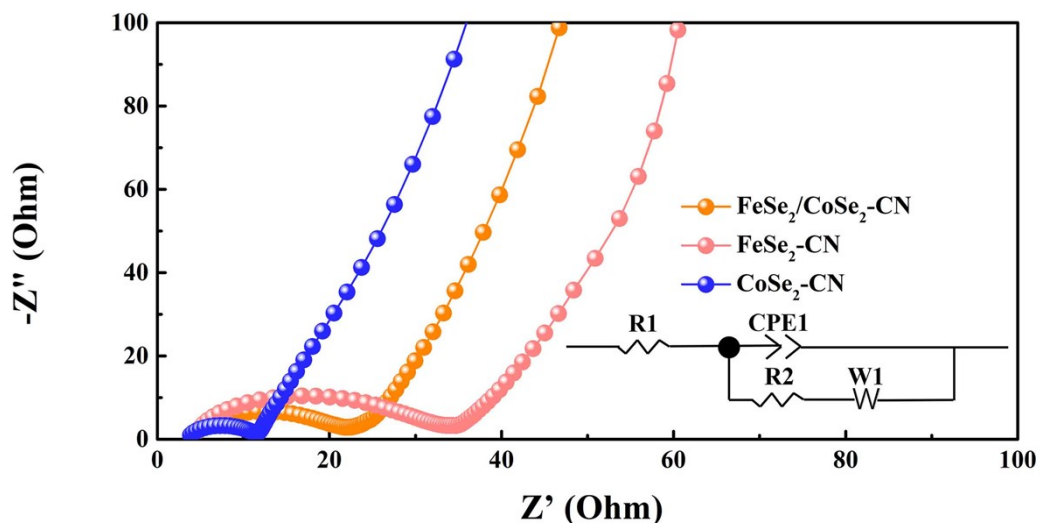


**Figure S17.** Nyquist plots of the FeSe<sub>2</sub>-CN, CoSe<sub>2</sub>-CN and FeSe<sub>2</sub>/CoSe<sub>2</sub>-CN (Inset is the corresponding equivalent circuit).

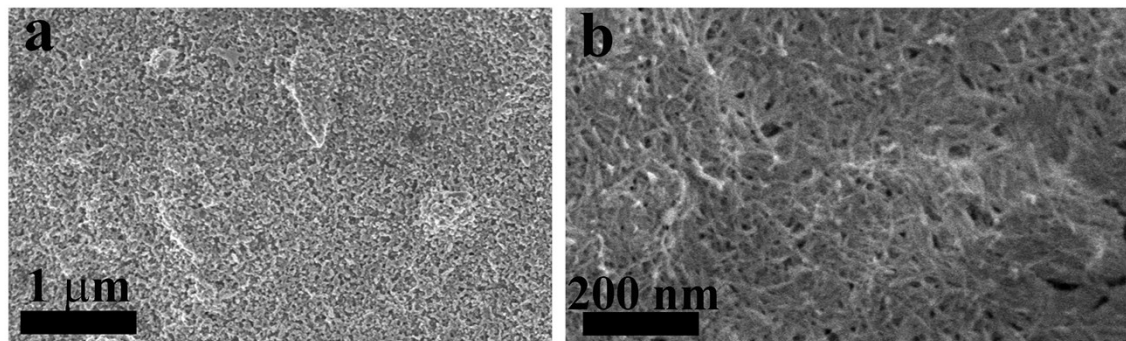


**Figure S18.** SEM images of FeSe<sub>2</sub>/CoSe<sub>2</sub>-CN after 50 cycles.

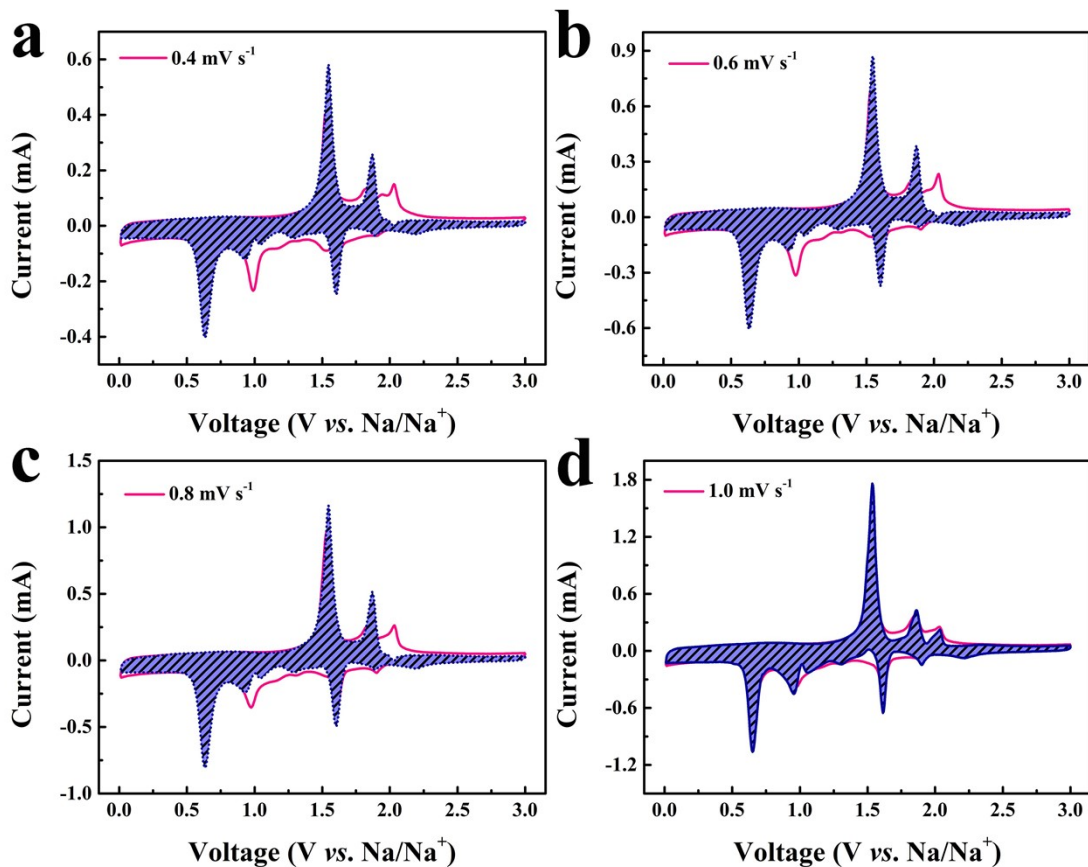


**Figure S19.** Capacitive contribution (shaded region) in CV curves (black line) under the scan rate of (a) 0.4 mV s<sup>-1</sup>, (b) 0.6 mV s<sup>-1</sup>, (c) 0.8 mV s<sup>-1</sup> and (d) 1.0 mV s<sup>-1</sup>.

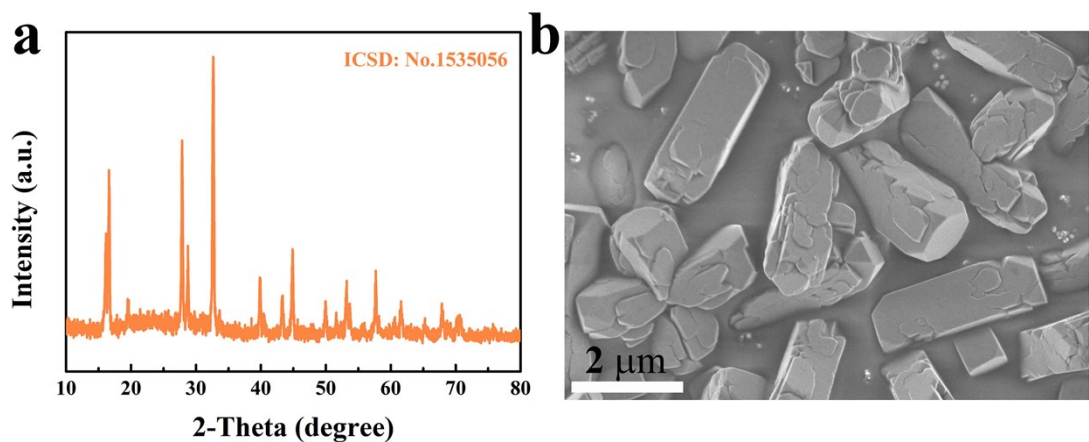


**Figure S20.** (a) XRD pattern of  $\text{Na}_3\text{V}_2(\text{PO}_4)_2\text{O}_2\text{F}$ . (b) SEM images of  $\text{Na}_3\text{V}_2(\text{PO}_4)_2\text{O}_2\text{F}$ .